Upper-bound solution for the stability of stone-facing embankments

Anne Sophie Colas, Jean Claude Morel, Denis Garnier

Upper-bound solution for the stability of stone-facing embankments

Colas, A. S. , Morel, J. C. and Garnier, D.

Original citation & hyperlink:
Colas, A. S. , Morel, J. C. and Garnier, D. (2016) Upper-bound solution for the stability of stone-facing embankments. *Materials and Structures*, volume 49 (10): 4279–4289
http://dx.doi.org/10.1617/s11527-015-0787-z

DOI 10.1617/s11527-015-0787-z
ISSN 1359-5997
ESSN 1871-6873

Publisher: Springer

The final publication is available at Springer via http://dx.doi.org/10.1617/s11527-015-0787-z

Materials and Structures manuscript No.
(will be inserted by the editor)

Upper-bound solution for the stability of stone-facing embankments

Anne-Sophie Colas · Jean-Claude Morel · Denis Garnier

Received: date / Accepted: date

Abstract An upper-bound solution for stone-facing embankments is developed to assess the stability of this type of structures. The embankment is treated as a cohesionless granular material whereas the facing is considered as composed of discrete stone blocks, laid dry one on the top of the other, complying with a Mohr-Coulomb interface law. This enables the assessment of the stability of the structure, solely resorting to its geometry, unit weight, and the friction angles of the embankment and facings. The model is finally used to assess the stability of an existing rockfill dam in the Pyrénées (France). Comparison with Distinct Element Method results and parametric analyses prove the robustness of the model on this case study.

Keywords Masonry facing · embankment · rockfill dam · dyke · upper-bound solution

1 Introduction

Embankments are hydraulic structures built to retain – called dams, or prevent – called dykes, water. They are generally made of earthfill or rockfill, covered with concrete, asphalt or masonry. These structures are difficult to model considering the heterogeneous nature of the material composing the embankment and the interface with its facing. Indeed, the loadings acting on the structure are complex:

A-S. Colas
Université Paris-Est, Ifsttar, MAST, SDOA
14-20 boulevard Newton, F-77447 Marne-la-Vallée cedex 2
E-mail: anne-sophie.colas@ifsttar.fr

J-C. Morel
Université de Lyon, ENTPE, LTDS (UMR 5513)
rue M. Audin, F-69518 Vaulx-en-Velin cedex
Present address: School of Energy, Construction and Environment. Centre of Low Impact buildings. Faculty of Engineering, Environment & Computing. Coventry University.

D. Garnier
Université Paris-Est, ENPC, Laboratoire Navier
6-8 avenue Blaise Pascal, F-77455 Marne-la-Vallée cedex 2

in addition to the unit weight, water action and even seismic risks should be taken in consideration. In this study, it has been decided to concentrate on a static analysis of masonry facing embankments.

Only few studies are dedicated to stone-facing embankment structures: they concentrate on masonry rockfill dams and resort to Distinct Element Method (DEM) (Deluzarche 2004; Deluzarche and Cambou 2006; Tran et al 2009; Bretas et al 2013, 2014). DEM has been developed to deal with discontinuous media, which are treated as an assembly of elements linked with contact interactions. In these studies, rockfill is modelled as composed of discrete blocks, with the objective to evaluate the safety of the structure. These studies provide exhaustive information on the behaviour of stone-facing rockfill dams at failure but require quantitative and qualitative information on the mechanical properties of the constituent materials, and can prove time-consuming.

The model presented here resorts to yield design theory. Yield design relies on the compatibility between the equilibrium of the structure under consideration and the resistance of its constituent materials in order to formulate a rigorous analytic expression of the upper-bound solution to its stability problems. It has been already used to model jointed rock mass (Bekaert et al 1998) and masonry retaining walls (Colas et al 2010a, 2013). The paper focuses on the application of this theory to the specific modelling of stone-facing embankments. First, the model is introduced and an analytical expression of the upper-bound solution for stone-facing embankments is presented. A case study is proposed, consisting in the structural evaluation of an existing dam. Finally, comparison with DEM results and parametric analyses are undertaken to assess the robustness of the model.

2 Analytic upper-bound solution for stone-facing embankment

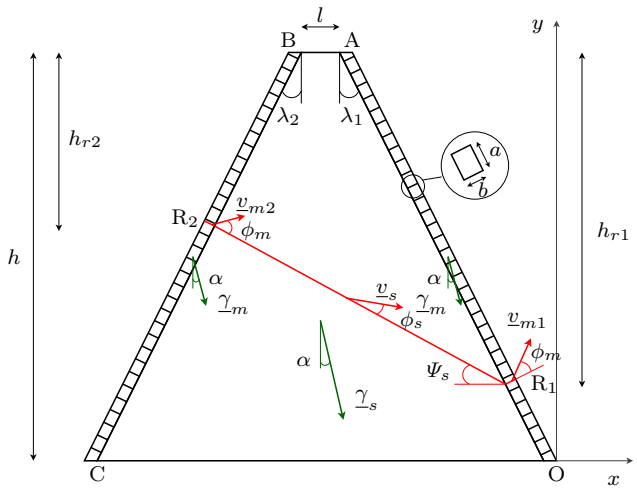

Fig. 1 Yield design upper-bound approach of a stone-facing embankment submitted to a rotation of gravity of angle α.

2.1 Introduction to yield design principles

According to yield design theory (Salençon 1990, 2013), the stability of a structure is based on the compatibility between static equilibrium under prescribed loading and strength verification at any point of its constituent materials. Two approaches have been implemented in this framework:

- the static approach, which consists in finding stress fields $\underline{\underline{\sigma}}$ in the strength domain G to provide a lower estimation of the extreme loading domain K:

$$\underline{\underline{\sigma}} \in G \Rightarrow \underline{Q} \in K \tag{1}$$

- the kinematic approach, which boils down to dualizing the static approach through the principle of virtual works to provide an upper-bound estimation of the extreme loading :

$$\underline{Q} \in K \Rightarrow \mathcal{P}^{\mathrm{e}} \leq \mathcal{P}^{\mathrm{rm}} = \int_{\mathcal{V}} \pi(\underline{\underline{d}})\, \mathrm{d}\mathcal{V} + \int_{\mathcal{S}} \pi(\underline{n}, [\![\underline{v}]\!])\, \mathrm{d}\mathcal{S} \tag{2}$$

where $\pi(\underline{\underline{d}})$ and $\pi(\underline{n}, [\![\underline{v}]\!])$ are the support functions of the strength domain G defined by:

$$\pi(\underline{\underline{d}}) = \sup_{\underline{\underline{\sigma}} \in G} \left\{ \underline{\underline{\sigma}} : \underline{\underline{d}} \right\} \tag{3}$$

$$\pi(\underline{n}, [\![\underline{v}]\!]) = \sup_{\underline{\underline{\sigma}} \in G} \left\{ \underline{\underline{\sigma}} \,.\, \underline{n} \,.\, [\![\underline{v}]\!] \right\} \tag{4}$$

2.2 Geometrical and physical characteristics

The static approach consists in finding stress fields ensuring the previous condition, thus giving a lower estimation of the extreme loading. The kinematic approach, which can be derived by dualizing the static approach through the principle of virtual work, provides an upper-bound estimation of the extreme loading

Geometry. The structure (Fig. 1) is composed of an embankment of height h and thickness at the top l. The structure will be treated in plane strain. The cross-section of the embankment has a trapezoidal shape: downstream slope is noted as $f_1 = \tan\lambda_1$ and upstream slope is noted as $f_2 = \tan\lambda_2$, where λ_1 and λ_2 are respectively the slope inclination of the downstream and upstream faces. Each slope is faced with a masonry cover composed of rectangular blocks of height a and thickness b, which are built dry with their bed joint normal to the face slope.

Loading. The system is solely subjected to the unit weight of its constitutive materials, which will be noted as $\underline{\gamma}_s$ for the embankment and $\underline{\gamma}_m$ for the masonry face. The influence of gravity is tested not by increasing its norm, but by inclining its direction from the vertical at an angle α. Indeed the introduction of a horizontal component of the body forces in the loading constitutes a first step towards the quasi-static approach of seismic problems; indeed, a vertical component may be added, using a lower unit weight of the constitutive materials. Considering

this angle of inclination α, the embankment and the stone-facing unit weights are written:

$$\underline{\gamma}_s = \gamma_s \sin\alpha \, \underline{x} - \gamma_s \cos\alpha \, \underline{y} \tag{5}$$
$$\underline{\gamma}_m = \gamma_m \sin\alpha \, \underline{x} - \gamma_m \cos\alpha \, \underline{y} \tag{6}$$

Resistance. The embankment is represented by a pulverulent material resorting to Mohr-Coulomb strength criterion. The support function associated to this criterion only depends on the friction angle of the material ϕ_s, the dilatancy angle being equal to ϕ_s, and can be found in Salençon (1990, 2013):

$$\pi\left(\underline{n}_s \, , [\![\underline{v}_s]\!]\right) = 0 \tag{7a}$$
$$\text{if } [\![\underline{v}_s]\!] \, . \, \underline{n}_s \geq |[\![\underline{v}_s]\!]| \, \sin\phi_s \tag{7b}$$

The blocks composing the stone-facing are considered as infinitely resisting. The joints are governed by a purely frictional Mohr-Coulomb criterion, depending on the friction angle of the stones ϕ_m. The support function of the joints is given by Salençon (1990, 2013):

$$\pi(\underline{n} \, , \underline{V}) = 0 \tag{8a}$$
$$\text{if } \underline{V}_n \geq |\underline{V}_t| \, \tan\phi_m \tag{8b}$$

where $\underline{V}$ denotes the velocity jump between two blocks of the stone-facing.

The same Mohr-Coulomb law is applied to the interface between the embankment and the stone-facing, with the frictional interface angle noted as δ:

$$\pi(\underline{n} \, , \underline{V}) = 0 \tag{9a}$$
$$\text{if } \underline{V}_n \geq |\underline{V}_t| \, \tan\delta \tag{9b}$$

where $\underline{V} = \underline{v}_m - \underline{v}_s$ denotes the velocity jump between the embankment and the stone-facing.

The value of the friction angle δ at the interface depends upon the choice of the material and the constructional arrangements between the embankment and the facing:

- $\delta = \phi_s$, if the material composing the embankment is laid loose with the stone-facing blocked on the embankment;
- $\delta = \phi_m$, if the embankment is faced, and the stone-facing less frictional than the embankment.

With these definitions of the loading and resistance parameters, it can be noted that the stability domain of the structure is necessarily a convex cone, with its apex at the origin and its geometry depending on the maximum load inclination α, in the plane of the loading parameters $\underline{\gamma}_m$ and $\underline{\gamma}_s$.

2.3 Definition of virtual velocity fields

In the framework of yield design kinematic approach, the ultimate loading is given by the minimum value over all the kinematically admissible failure mechanisms. Nevertheless, as it is impossible to explore them all, this approach solely provides an upper-bound of the ultimate loading. It has been decided here to explore rigid body translation mechanisms. A failure line is drawn through the embankment, delimiting a motionless lower part from the upper part translating at a constant velocity field noted $\underline{v}_s$ for the embankment, $\underline{v}_{m1}$ for the downstream stone-facing, and $\underline{v}_{m2}$ for the upstream stone-facing (Fig. 1). This mechanism has been chosen for its simplicity and its correspondence with experimental results on retaining structures (Villemus et al 2007; Colas et al 2010b), and DEM results (Deluzarche 2004; Deluzarche and Cambou 2006; Tran et al 2009) on rockfill dams.

The failure line crossing the embankment can be defined by its origin R_1 on the downstream stone-facing [OA], quoted with its height h_{r1}, and its extremity R_2 on the upstream stone-facing [BC], quoted with its height h_{r2}. The study is generalised to the case of a failure line extremity R_2 situated in the top of the embankment [AB]; the distance AR_2 is then noted l_r. Considering the discrete character of the stone-facing, it can be noticed that h_{r1} and h_{r2} cannot reach every value between 0 and h as they correspond to an integer number of blocks n_{r1} and n_{r2}, so that:

$$\begin{aligned} h_{r1} &= n_{r1} a \cos\lambda_1 \\ h_{r2} &= n_{r2} a \cos\lambda_2 \end{aligned} \tag{10}$$

Based on these kinematic variables, the angle of inclination Ψ_s of the failure line can be defined as:

$$\tan\Psi_s = \frac{h_{r1} - h_{r2}}{l_r + h_{r1} f_1 + h_{r2} f_2} \tag{11}$$

with $\begin{vmatrix} l_r = l & \text{if } R_2 \in [BC] \\ h_{r2} = 0 & \text{if } R_2 \in [AB] \end{vmatrix}$

The velocity field $\underline{v}_s$ has to comply with the relevancy conditions of the resisting criterion chosen for the embankment (7b). Thus, considering this condition, $\underline{v}_s$ can be written as :

$$\underline{v}_s = v_s \cos(\Psi_s - \phi_s)\, \underline{x} - v_s \sin(\Psi_s - \phi_s)\, \underline{y} \tag{12}$$

The velocity fields $\underline{v}_{m1}$ and $\underline{v}_{m2}$ have to comply with the relevancy conditions of the resisting criterion chosen for the stone blocks (8b). Thus, considering this condition, $\underline{v}_{m1}$ and $\underline{v}_{m2}$ can be written as :

$$\underline{v}_{m1} = v_{m1} \cos(\phi_m + \lambda_1)\, \underline{x} + v_{m1} \sin(\phi_m + \lambda_1)\, \underline{y} \tag{13}$$

$$\underline{v}_{m2} = v_{m2} \cos(\phi_m - \lambda_2)\, \underline{x} + v_{m2} \sin(\phi_m - \lambda_2)\, \underline{y} \tag{14}$$

Considering the upstream facing has no stabilizing influence on the embankment stability, it has been decided to take v_{m2} equal to 0 when its vertical component is positive that is to say:

$$\underline{v}_{m2} = \underline{0} \quad \text{if } \underline{\gamma}_m \cdot \underline{v}_{m2} \leq 0 \tag{15}$$

The interface between the embankment and the masonry facing relies on a Mohr-Coulomb criterion with the relevancy condition on the velocity jump $\underline{V}_i =$

$\underline{v}_{mi} - \underline{v}_s$ exposed in (9b). Thus, considering this condition, $\underline{v}_{m1}$, $\underline{v}_{m2}$ and $\underline{v}_s$ are related by (Fig. 2):

$$v_{m1} = \frac{\cos(\Psi_s - \phi_s - \delta + \lambda_1)}{\cos(\phi_m + \delta)}\, v_s \tag{16}$$

$$v_{m2} = \frac{\cos(\Psi_s - \phi_s - \lambda_2 + \delta)}{\cos(\phi_m - \delta)}\, v_s \tag{17}$$

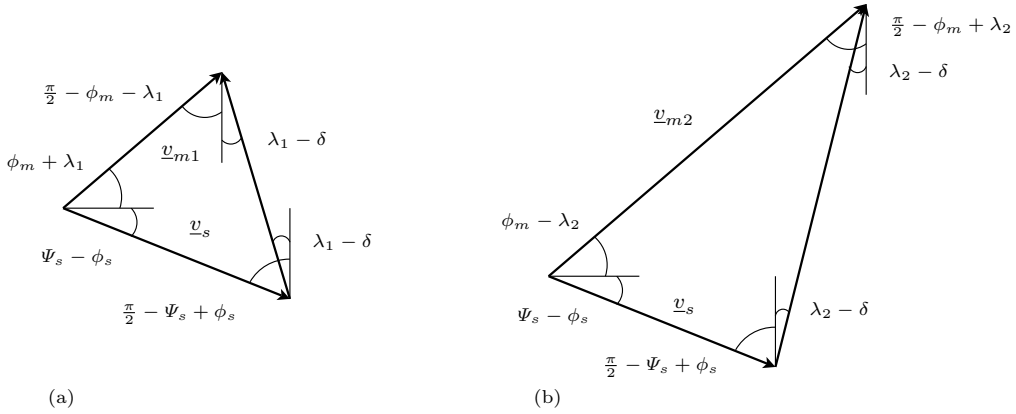

Fig. 2 Velocity jump conditions at the interface between the embankment and the downstream stone-facing (a) or upstream stone-facing (b).

2.4 Upper-bound limit of stability of masonry dams

The stability of the structure is assessed using yield design upper-bound approach, with the objective to determine the inclination of gravity $\alpha^{\max}$ which leads to the failure of the embankment.

The work of the external forces $\mathcal{P}^e$ falls into three parts, corresponding to the work in the embankment $\mathcal{P}^e_s$, and the work of the downstream $\mathcal{P}^e_{m1}$ and upstream $\mathcal{P}^e_{m2}$ stone-facing.

For simplification, the following notations will be assumed :

$$\xi_s = \Psi_s - \phi_s \tag{18a}$$

$$\xi_1 = \phi_m + \lambda_1 \tag{18b}$$

$$\xi_2 = \phi_m - \lambda_2 \tag{18c}$$

$$\zeta_{11} = \Psi_s - \phi_s - \delta + \lambda_1 \tag{18d}$$

$$\zeta_{12} = \phi_m + \delta \tag{18e}$$

$$\zeta_{21} = \Psi_s - \phi_s - \lambda_2 + \delta \tag{18f}$$

$$\zeta_{22} = \phi_m - \delta \tag{18g}$$

Considering equations (5) and (12), the work of the external forces in the embankment $\mathcal{P}_s^e$ can be written as:

$$\mathcal{P}_s^e = \int_{\mathcal{V}_s} \underline{\gamma}_s \cdot \underline{v}_s \, \mathrm{d}\mathcal{V} \tag{19}$$

$$\mathcal{P}_s^e = \frac{\gamma_s v_s}{2} \sin(\alpha + \xi_s) \left[(h_{r1} + h_{r2})\, l + (f_1 + f_2)\, h_{r1} h_{r2} \right]$$

Considering equations (6), (13) and (16), the work of the external forces in the downstream stone-facing $\mathcal{P}_{m1}^e$ can be written as:

$$\begin{aligned} \mathcal{P}_{m1}^e &= \int_{\mathcal{V}_{m1}} \underline{\gamma}_m \cdot \underline{v}_{m1} \, \mathrm{d}\mathcal{V} \\ \mathcal{P}_{m1}^e &= \gamma_m b h_{r1} v_s \, \frac{\cos\zeta_{11} \sin(\alpha - \xi_1)}{\cos\zeta_{12} \cos\lambda_1} \end{aligned} \tag{20}$$

Similarly, considering equations (6), (14) and (17), the work of the external forces in the upstream stone-facing $\mathcal{P}_{m2}^e$ can be written as:

$$\begin{aligned} \mathcal{P}_{m2}^e &= \int_{\mathcal{V}_{m2}} \underline{\gamma}_m \cdot \underline{v}_{m2} \, \mathrm{d}\mathcal{V} \\ \mathcal{P}_{m2}^e &= \gamma_m b h_{r2} v_s \, \frac{\cos\zeta_{21} \sin(\alpha - \xi_2)}{\cos\zeta_{22} \cos\lambda_2} \end{aligned} \tag{21}$$

The final expression of $\mathcal{P}^e$ is thus given by the sum of (19), (20) and (21):

$$\mathcal{P}^e = \mathcal{P}_{m1}^e + \mathcal{P}_{m2}^e + \mathcal{P}_s^e \tag{22}$$

The maximum resisting work is also given by the sum of the work in the embankment $\mathcal{P}_s^{rm}$, and the work of the downstream $\mathcal{P}_{m1}^{rm}$ and upstream $\mathcal{P}_{m2}^{rm}$ stone-facings. Yet, each maximum resisting work falls to 0 as the corresponding support functions equal 0, referring to equations (7a), (8a) and (9a), thus:

$$\mathcal{P}^{rm} = 0 \tag{23}$$

Based on the principle of virtual work, the yield design upper-bound theorem states that the work of the external forces has to remain lower than the maximum resisting work to ensure the stability of the structure:

$$\mathcal{P}^e \leq \mathcal{P}^{rm} \tag{24}$$

$$\alpha \leq \arctan \frac{2\gamma_m\, b\big(C_1 \sin\xi_1 + C_2 \sin\xi_2\big) - \gamma_s C_s \sin\xi_s}{2\gamma_m b\big(C_1 \cos\xi_1 + C_2 \cos\xi_2\big) + \gamma_s C_s \cos\xi_s} \tag{25}$$

where C_1, C_2 and C_s are:

$$\begin{aligned} C_1 &= \frac{\cos(\Psi_s - \phi_s - \delta + \lambda_1)}{\cos\lambda_1 \cos(\phi_m + \delta)}\, h_{r1} \\ C_2 &= \frac{\cos(\Psi_s - \phi_s - \lambda_2 + \delta)}{\cos\lambda_2 \cos(\phi_m - \delta)}\, h_{r2} \\ C_s &= (h_{r1} + h_{r2})\, l_r + (f_1 + f_2)\, h_{r1} h_{r2} \end{aligned} \tag{26}$$

Finally, the minimisation of the right member of the inequality (25), noted as $\alpha^{\lim}$, with respect to the kinematic parameters n_{r1} and n_{r2} provides an upper-bound limit value of the rotation of gravity α ensuring the collapse of the embankment:

$$\alpha^{\max} = \min_{n_{r1}, n_{r2}, l_r} \left\{ \alpha^{\lim}\Big(h_{r1}, h_{r2}, l_r, \Psi_s\Big) \right\} \tag{27}$$

2.5 Consideration of water pressure

In case the model deals with embankment dams, an additional development is necessary to take into account the action of water on the structure. In order to ensure the impermeability of the dam, the upstream face is usually covered by an impervious concrete layer (see for instance Fig. 3b). The action of water will thus be modelled by a hydrostatic pressure applied on the upstream face.

Considering a water reserve of height h_w behind the dam, the work of the external forces P_e (22) is amended with a fourth term $\mathcal{P}_w^e$ representing the work of the water pressure:

$$\mathcal{P}^e = \mathcal{P}_{m1}^e + \mathcal{P}_{m2}^e + \mathcal{P}_s^e + \mathcal{P}_w^e \tag{28}$$

where P_w^e is:

$$\begin{aligned} P_w^e &= \int_{h-h_{r2}}^{h_w} \underline{p}_w \cdot \underline{v}_{m2} \, \frac{\mathrm{d}x_2}{\cos\lambda_2} \\ P_w^e &= \frac{\gamma_w v_{m2} \cos\phi_m}{2\cos\lambda_2} \left(h_w - h + h_{r2}\right)^2 \end{aligned} \tag{29}$$

if $h_w \leq h - h_{r2}$, and $P_w^e = 0$ otherwise.

The maximum resisting work remains (23), with the same conditions on the virtual velocity fields.

This provides a new expression of $\alpha^{\max}$ depending on the previous parameters plus the unit weight of water $\underline{\gamma}_w$ and the height of the reservoir h_w.

3 Application to a rockfill dam case study

An application of the model is undertaken on a real case study, taken from Deluzarche (2004): it consists in a rockfill embankment dam situated in the department of Hautes-Pyrénées (France). This dam, dated from the middle of the XX$^{\text{th}}$ century, is composed of a 20 m high granitic rockfill embankment covered with a stone-facing on each face (Fig. 3).

Based on the information given by Deluzarche (2004), geometrical and physical characteristics have been defined and reported in Table 1.

The model exposed in section 2 is used to assess the stability of the dam. The parameters given in Table 1 are reported in (27) in order to calculate the maximum inclination of gravity the dam can bear.

Considering the dam on its own, the failure is ensured for a rotation of gravity:

$$\alpha^{\max} = 37.1^\circ \tag{30}$$

(a)

(b)

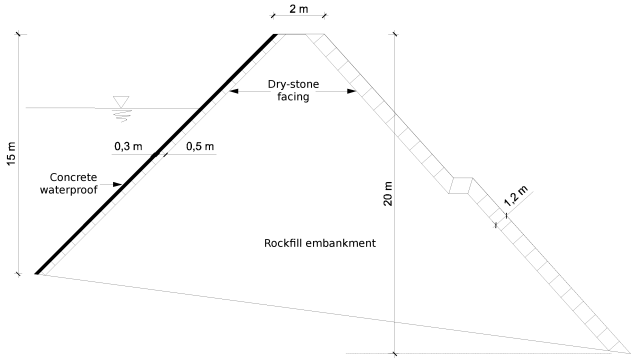

Fig. 3 Full-scale dam case study (source EDF): view of the downstream stone-facing (a) and schematic view of the section (b).

Table 1 Geometrical and physical parameters selected for the study of a full-scale dam.

Parameters	Symbol	Value	Unit
Dam height	h	20.0	m
Dam thickness at the top	l	1.0	m
Dam downstream slope	λ_1	45	°
Dam upstream slope	λ_2	45	°
Stone block height	a	0.3	m
Stone block thickness	b	1.2	m
Water height	h_w	20.0	m
Rockfill unit weight	γ_s	18.3	kN/m^3
Rockfill friction angle	ϕ_s	37.7	°
Stone-facing unit weight	γ_m	21.0	kN/m^3
Stone block friction angle	ϕ_m	35.0	°
Interface friction angle	δ	35.0	°

It can be noticed that this value is reached for $n_{r1} = 0$ and $n_{r2} = 49$, corresponding to a failure line starting from the toe of the dam and ending in the upstream stone-facing with an angle $\Psi_s = 26°$. The kinematic parameters involved in the upper

bound approach may be virtual, they yet provide an indication on the possible failure mechanism.

For the case in which the reservoir is full, the failure is ensured for a rotation of gravity:

$$\alpha^{\max} = 31.4^{\circ} \tag{31}$$

This value is lower than the rotation of gravity needed to collapse the dam without retaining water (30). Nevertheless, the action of water on the stability of the structure remains moderate. The failure of the dam is reached for $n_{r1} = 0$ and $n_{r2} = 37$, corresponding to a failure line starting from the toe and developing with an angle $\Psi_s = 20^{\circ}$.

4 Comparison with DEM results

Deluzarche (2004) analyses the stability of this dam using a Distinct Element Method model of rockfill developed for the study. He has undertaken independent and combined tests on the mechanical properties of the rockfill and the stone-facing, and the loadings, in various configurations of the dam. In this study, the authors concentrate on the tests of:

- the presence of stone-facing;
- the presence of water;
- the diminution of the rockfill friction angle ϕ_s;
- the diminution of the stone friction angle ϕ_m;
- the effect of a rotation α_0 of gravity.

The tests undertaken by Deluzarche have been reproduced using yield design and compared to the DEM results; tests and results are reported in Table 2.

Table 2 Comparison with DEM simulations taken from Deluzarche (2004) on a full-scale dam: yield design failure is appreciated with the previously exposed model and the additional rotation of gravity $\alpha^{\mathrm{f}} = \alpha^{\max} - \alpha_0$ needed for failure is given into brackets.

Facing	Water	ϕ_s (°)	ϕ_m (°)	α_0 (°)	DEM failure	YD failure (α^{f})
No	No	37.7	–	0	YES	YES
No	No	45.6	–	0	NO	NO (0.6)
Yes	No	37.7	35.0	0	NO	NO (37.1)
Yes	Yes	37.7	35.0	0	NO	NO (31.4)
Yes	Yes	30.4	26.6	0	NO	NO (16.2)
Yes	Yes	21.2	5.7	0	YES	YES
Yes	Yes	37.7	35.0	5	NO	NO (26.4)
Yes	Yes	37.7	35.0	10	YES	NO (21.4)
Yes	Yes	37.7	35.0	20	YES	NO (11.4)

Comparing yield design and DEM results (Tab. 2), it can be seen that the two methods provide close results, considering the influence of the facing and the water reserve. The stabilising role of stone-facing is more important in yield design simulation as structures without stone-facing are unstable or likely to become for $\phi_s = 45.6^{\circ}$. This is consistent with the definition of an upper-bound solution in case of yield design.

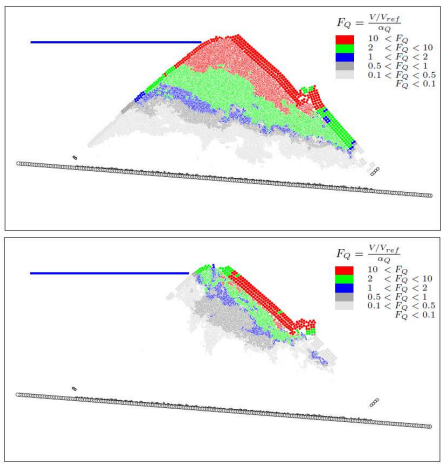

Fig. 4 Iso-values of velocities on DEM simulations for a rotation of gravity of 20° (top) and 10° (bottom) from Deluzarche (2004).

Yet, the effect of a rotation of gravity is much more impacting in DEM simulations. For an angle of rotation $\alpha = 10°$, the dam is still stable in yield design, as it fails for $\alpha^{\max} = 31.4° > \alpha_0$, whereas DEM simulations show an instability located in the upper part of the stone-facing. However, the reduced zone of instability highlighted in DEM suggests that the whole stability of the dam is not compromised (Fig. 4). For $\alpha_0 = 20°$, the dam is quite close to failure in yield design – about 10° left before failure. In DEM simulations, a failure line, starting from the upper third of the upstream face to the half of the downstream face, develop in the dam. This difference can be accounted for by the upper-bound character of the yield design solution, which leads to an overestimation of the maximum angle of failure. The failure line observed in DEM simulations (Fig. 4) suggests that the difference can also be due to the discontinuity in the downstream face of the dam, called the risberm, which is not taken into account in yield design simulation. More DEM calculations would be necessary to precise the conclusions.

5 Parametric analysis

The sensitivity of the model is addressed by a parametric analysis on different characteristics of the dam. This enables the identification of the most influential parameters, which value have to be measured carefully. This also highlights the part of constructional arrangements in the stability of the construction, and can thus provide information on the elements which should be paid attention to during the inspection of an existing dam.

5.1 Influence of the water height

The first parametric analysis focuses on the influence of the water impoundment on the dam. Fig. 5a shows the evolution of the failure angle of inclination $\alpha^{\max}$

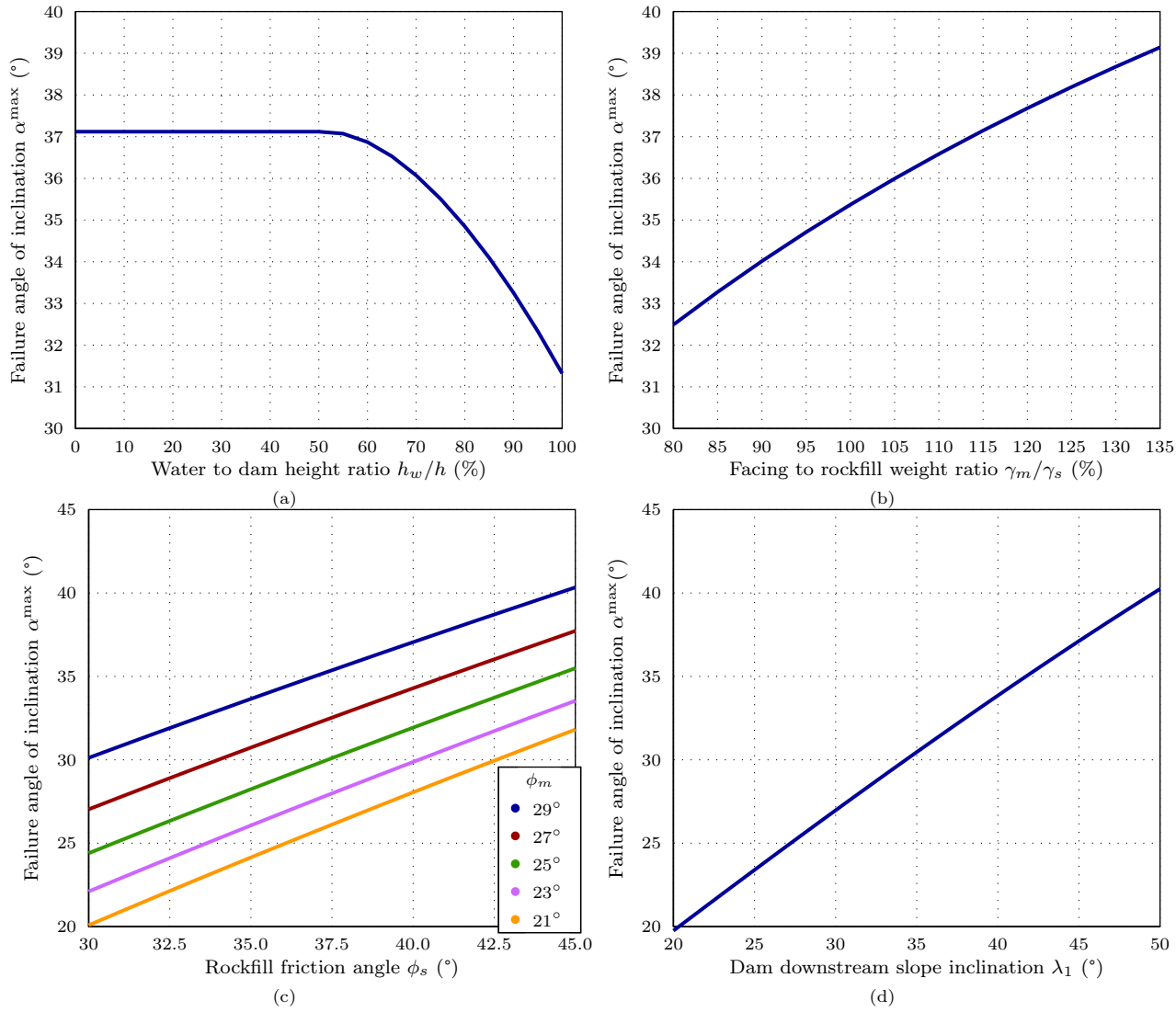

Fig. 5 Evolution of the failure angle of inclination $\alpha^{\max}$ depending on the water to dam height ratio h_w/h (a), the facing to rockfill weight ratio γ_m/γ_s (b), the friction angle of the rockfill ϕ_s and the stone-facing ϕ_m (c), and the dam downstream slope inclination λ_1 (d).

with the filling of the dam. It can be seen that the water reserve has no influence on the dam stability when the level is above 50% of the dam height. This is due to the slope of the optimal internal failure line in the dam which ends above half of the upstream face. Then, the water reserve leads to a reduction of the stability of the dam, even though, as already mentioned in section 3, this reduction remains moderate.

The following parametric analyses concentrate on the dam on its own, without water reserve.

5.2 Influence of the stone-facing and rockfill weights

Rockfill dams are gravity structures, and the weights of the constituent materials of the dam have a great influence on its behaviour. Fig. 5b shows the evolution of failure angle of inclination $\alpha^{\max}$ depending on the facing to rockfill weight ratio γ_m/γ_s. The stability of the dam increases with the weight ratio, proving the important role of the dry-stone facing.

5.3 Influence of the friction angles of the rockfill and the stone-facing

The influence of the resisting characteristics can be evaluated by plotting the evolution of the failure angle of inclination of the dam $\alpha^{\max}$ depending on the rockfill friction angle ϕ_s for different values of ϕ_m, the stone block friction angle (Fig. 5c). It can be noticed that the stability of the structure increases with the friction angle of the rockfill and the stone. The stone and the rockfill friction angles stand for an important part of the stability: thus, they should be measured precisely ($\pm 2^\circ$) to ensure an accurate assessment of the structure.

5.4 Influence of the friction angle at the interface

The interface between the rockfill and its stone-facing is considered as purely frictional, complying with a Mohr-Coulomb law of friction angle δ. In a first approach, it has been decided to take the friction angle of the interface equal to the friction angle of the blocks composing the stone-facing $\delta = \phi_m$. This value seems relevant for rockfill built carefully, with regular faces, as explained in section 2.2. However, for loose rockfill it seems better to use the friction angle of the rockfill $\delta = \phi_s$. In this case, the maximum friction angle equals:

$$\alpha^{\max} = 39.0^\circ \tag{32}$$

This represents an increase of 5% of the stability compared to the value obtained with $\delta = \phi_s$ (30). In this case study, the interface friction angle has a moderate effect on the stability of the structure; this can be accounted for by the little difference between the two friction angles, which is common situation as rockfill and facing are often built with the same material.

5.5 Influence of the dam downstream slope inclination

The most remarkable specificity of this dam is the geometry of the downstream-face, which angle with the horizontal proves higher than the friction angle of the rockfill. The influence of this geometric parameter is evaluated in Fig. 5d, representing the evolution of the failure angle of inclination $\alpha^{\max}$ depending on the dam downstream slope inclination λ_1. The graph consistently shows that the stability of the dam increases with its downstream slope. Besides, it can be seen that, even with a lower downstream slope, the dam still proves stable, even close to failure.

5.6 Influence of the orientation of the stone blocks

In the model previously exposed, blocks are considered as rectangular, with bed joints normal to the embankment slope. It can prove interesting to evaluate the influence of the block inclination, considering blocks are no longer rectangles but parallelograms of height a and thickness b with their bed joints parallel to the foundation. The formulas established in section 2 remain valid, except for $\underline{v}_{m1}$ et $\underline{v}_{m2}$:

$$\underline{v}_{m1} = v_{m1} \cos\phi_m \ \underline{x} + v_{m1} \sin\phi_m \ \underline{y} \tag{33}$$

$$\underline{v}_{m2} = v_{m2} \cos\phi_m \ \underline{x} + v_{m2} \sin\phi_m \ \underline{y} \tag{34}$$

and their relations with the virtual velocity in the embankment :

$$v_{m1} = \frac{\cos(\Psi_s - \phi_s - \delta + \lambda_1)}{\cos(\phi_m + \delta - \lambda_1)} \, v_s \tag{35}$$

$$v_{m2} = \frac{\cos(\Psi_s - \phi_s - \lambda_2 + \delta)}{\cos(\phi_m + \lambda_2 - \delta)} \, v_s \tag{36}$$

The expression of the maximum angle of inclination $\alpha^{\max}$ is:

$$\alpha \leq \arctan \frac{2\gamma_m b \sin\phi_m \left(K_1 + K_2\right) - \gamma_s C_s \sin\xi_s}{2\gamma_m b \cos\phi_m \left(K_1 + K_2\right) + \gamma_s C_s \cos\xi_s} \tag{37}$$

where K_1, K_2 and C_s are:

$$\begin{aligned} K_1 &= \frac{\cos(\Psi_s - \phi_s - \delta + \lambda_1)}{\cos(\phi_m + \delta - \lambda_1)} \, h_{r1} \\ K_2 &= \frac{\cos(\Psi_s - \phi_s - \lambda_2 + \delta)}{\cos(\phi_m + \lambda_2 - \delta)} \, h_{r2} \\ C_s &= (h_{r1} + h_{r2}) \, l_r + (f_1 + f_2) \, h_{r1} h_{r2} \end{aligned} \tag{38}$$

Thus, the expression of the maximum angle of inclination $\alpha^{\max}$ can be deduced from the minimization of the previous expression towards $h_{r1} = n_{r1} a$, $h_{r2} = n_{r2} a$ and l_r:

$$\alpha^{\max} = \min_{n_{r1}, n_{r2}, l_r} \left\{ \alpha^{\lim}\Big(h_{r1}, h_{r2}, l_r, \Psi_s\Big) \right\} \tag{39}$$

Considering the parameters in Table 1, the maximum value of $\alpha^{\max}$ is :

$$\alpha^{\max} = 13.1^\circ \tag{40}$$

Comparison of this value with (30) shows a decrease in stability of 60%, proving the importance of joint orientation for an equivalent volume of stone. This result is particularly interesting for inspection of existing dams, as observing the rotation of the stone-facing bed joints denotes a loss of stability of the structure.

5.7 Influence of stone-facings

The influence of the upstream and downstream stone-facings on rockfill dams stability have finally been tested in the model.

Removing the upstream stone-facing of the dam provides a failure angle of inclination :

$$\alpha^{\max} = 39.6^{\circ} \tag{41}$$

The rockfill dam shows slightly the same stability with (30) or without upstream stone-facing, meaning that this cover could be neglected in further calculation to simplify the model.

Considering there are no stone-facings, the dam is unstable. This result is consistent with the daring geometry of the embankment, which slope is higher than the friction angle of the material constituting the rockfill. This proves the importance of the downstream stone-facing in the stability of the rockfill dam as it can bear a rotation of gravity of 37.1° with stone-facing (40).

6 Conclusions and perspectives

In this article, an upper-bound solution to assess the stability of stone-facing embankments is developed. The model enables the analytic calculation of the structure, solely based on its geometry, unit weight and yield criterion. Then, the model is tested on a case study consisting in the structural evaluation of an existing dam. The model is compared to DEM simulations undertaken by Deluzarche (2004). Yield design provides an upper-bound solution for the stability of the dam, resorting on few parameters and requiring no calculation device or time, and thus proving an efficient tool to address structural evaluation problems on stone-facing embankments. Finally, a parametric analysis on this example proves the stabilising role of the stone-facing as well as the influence of the stone block orientation in the stability of the structure.

Acknowledgements This work is part of the national project PEDRA (ref. 10 MGC S 017) devoted to the study of vernacular masonry constructions. The authors would like to thank the French Ministry of Ecology, Sustainable Development and Energy for their financial support to this project.

List of symbols

α	angle of rotation of gravity
h	height of embankment
l	thickness at top of embankment
λ_1	front batter of embankment
λ_2	back batter of embankment
a	height of stone-facing blocks
b	thickness of stone-facing blocks
h_w	height of water reserve
γ_m	unit weight of stone-facing
γ_s	unit weight of embankment
ϕ_m	block friction angle
ϕ_s	embankment friction angle
δ	interface friction angle
$\mathcal{P}^e$	work of external forces
$\mathcal{P}^{rm}$	maximum resisting work
$\underline{v}_{m1}$	virtual velocity field in downstream stone-facing
$\underline{v}_{m2}$	virtual velocity field in upstream stone-facing
$\underline{v}_s$	virtual velocity field in embankment
h_{r1}	failure line downstream height
h_{r2}	failure line upstream height
Ψ_s	failure line angle
$\underline{\underline{\sigma}}$	stress field tensor
$\underline{\underline{d}}$	strain rate tensor
$\underline{Q}$	loading mode
$\underline{G}$	strength domain
K	extreme loading domain

References

Bekaert A, de Buhan P, Maghous S (1998) Failure design of jointed rock structures by means of a homogenization approach. Mechanics of Cohesive-Frictional Materials 3(13):207–228

Bretas EM, Lemos JV, Lourenço PB (2013) Hydromechanical analysis of masonry gravity dams and their foundations. Rock Mechanics and Rock Engineering 46(2):327–339

Bretas EM, Lemos JV, Lourenço PB (2014) A DEM based tool for the safety analysis of masonry gravity dams. Engineering Structures 59:248–260

Colas AS, Morel JC, Garnier D (2010a) 2D modelling of a dry joint masonry wall retaining a pulverulent backfill. International Journal for Numerical and Analytical Methods in Geomechanics 34(12):1237–1249

Colas AS, Morel JC, Garnier D (2010b) Full-scale field trials to assess dry-stone retaining wall stability. Engineering Structures 32(5):1215–1222

Colas AS, Morel JC, Garnier D (2013) Assessing the two-dimensional behaviour of dry-stone retaining walls by full-scale experiments and yield design simulation. Géotechnique 63(2):107–117

Deluzarche R (2004) Modélisation discrète des enrochements – application aux barrages. PhD thesis, École Centrale de Lyon

Deluzarche R, Cambou B (2006) Discrete numerical modelling of rockfill dams. International Journal for Numerical and Analytical Methods in Geomechanics 30(11):1075–1096

Salençon J (1990) An introduction to the yield design theory and its application to soil mechanics. European Journal of Mechanics - A/Solids 9(5):477–550

Salençon J (2013) Yield Design. Wiley-ISTE, London

Tran TH, Vénier R, Cambou B (2009) Discrete modelling of rock-ageing in rockfill dams. Computers and Geotechnics 36(1-2):264–275
Villemus B, Morel JC, Boutin C (2007) Experimental assessment of dry stone retaining wall stability on a rigid foundation. Engineering Structures 29(9):2124–2132